Rational Enantioselective Design of Chiral Heterobimetallic Single-Chain Magnets: Synthesis, Crystal Structures and Magnetic Properties of Oxamato-Bridged (MCuII)-Cu-II Chains (M=M...

ARTICLE *in* CHEMISTRY - A EUROPEAN JOURNAL · OCTOBER 2011

Impact Factor: 5.73 · DOI: 10.1002/chem.201101459 · Source: PubMed

CHEMISTRY
A EUROPEAN JOURNAL

DOI: 10.1002/chem.201101459

Rational Enantioselective Design of Chiral Heterobimetallic Single-Chain Magnets: Synthesis, Crystal Structures and Magnetic Properties of Oxamato-Bridged $M^{II}Cu^{II}$ Chains (M = Mn, Co)

Jesús Ferrando-Soria,[a] Danielle Cangussu,[b] Mercedes Eslava,[a] Yves Journaux,*[b, c] Rodrigue Lescouëzec,[b] Miguel Julve,[a] Francesc Lloret,*[a] Jorge Pasán,[d] Catalina Ruiz-Pérez,[d] Elsa Lhotel,[e] Carley Paulsen,[e] and Emilio Pardo*[b]

Abstract: A new series of neutral oxamato-bridged $M^{II}Cu^{II}$ chiral chains of general formula $[MCuL^{x}(S)_{m}(H_2O)_{n}]\cdot aS\cdot bH_2O$ [L^1 = (*M*)-1,1′-binaphthalene-2,2′-bis(oxamate) with M = Mn (**1a**) and Co (**1b**); L^2 = (*P*)-1,1′-binaphthalene-2,2′-bis(oxamate) with M = Mn (**2a**) and Co (**2b**)] and the analogous racemic chains of formula $[MCuL^{3}(S)_{m}(H_2O)_{n}]\cdot aS\cdot bH_2O$ [L^3 = 1,1′-binaphthalene-2,2′-bis(oxamate) with M = Mn (**3a**) and Co (**3b**)] have been prepared by reaction of the corresponding dianionic oxamatocopper(II) complex $[Cu(L^{x})]^{2-}$ with Mn^{2+} or Co^{2+} cations in either dimethylformamide (DMF) or dimethyl sulfoxide (DMSO). Solid circular dichroism (CD) spectra of the bimetallic chain compounds were recorded to establish their chiral and enantiomeric nature. They exhibit maximum positive and negative Cotton effects, each pair of enantiomeric chains being non-superimposable mirror images. The crystal structures of the $Mn^{II}Cu^{II}$ (**1a**–**3a**) and the $Co^{II}Cu^{II}$ (**1b** and **2b**) chain compounds were solved by single-crystal X-ray diffraction methods. Our attempts to obtain X-ray quality crystals of **3b** were unsuccessful. The values of the shortest interchain Mn···Mn and Co···Co distances are indicative of a good isolation of neighbouring chains in the crystal lattice, which is caused by the bulky aromatic ligand. Although all the $Mn^{II}Cu^{II}$ and $Co^{II}Cu^{II}$ chains exhibit ferrimagnetic behaviour ($-J_{MnCu}$ = 18.9–26.6 cm^{-1} and $-J_{CoCu}$ = 19.5–32.5 cm^{-1}), only the enantiopure $Co^{II}Cu^{II}$ chains (**1b** and **2b**) show slow magnetic relaxation at low temperatures (T_B = 0.6–1.8 K), which is a characteristic of single-chain magnets (SCMs) and is related to the magnetic anisotropy of the high-spin Co^{II} ion. Analysis of the SCM behaviour of **1b** and **2b**, based on Glauber's theory for an Ising one-dimensional system, shows a thermally activated mechanism for the magnetic relaxation (Arrhenius law dependence). The energy barriers (E_a) to reverse the magnetisation direction are 8.2 (**1b**) and 8.1 cm^{-1} (**2b**), whereas the pre-exponential factor (τ_0) is 1.9×10^{-8} (**1b**) and 6.0×10^{-9} s (**2b**). Interestingly, the racemic $Co^{II}Cu^{II}$ chain analogue, **3b**, showed no evidence of SCM behaviour.

Keywords: chirality · cobalt · copper · manganese · magnets

Introduction

The design and synthesis of multifunctional magnetic molecular materials (M_4) have become an outstanding area of research in recent years and have led to new possibilities in molecule-based magnetic materials.[1–6] This new class of materials possessing one or more independent physical properties in addition to the magnetic properties includes a great variety of often very different types of compounds. These can be classified into two main categories: one in which the magnetic properties can be tuned by the application of external stimuli (light, pressure or temperature), such as photomagnets[1] and spin-crossover materials,[2] and another in which two properties coexist in one material (dual-function materials), for example, magnetic conductors,[3] or more interesting but scarce, an interaction between the two properties to give a third, such as chiral magnets[4] that tentatively show magnetochiral dichroism.[5] The major goal in this field is to synthesise and explore the original properties of new classes of compounds that exhibit multifunctional properties

[a] J. Ferrando-Soria, M. Eslava, Prof. Dr. M. Julve, Prof. Dr. F. Lloret
Departament de Química Inorgànica
Instituto de Ciencia Molecular (ICMOL), Universitat de València
Paterna, 46980 València (Spain)
Fax: (+34) 96-354-4322
E-mail: francisco.lloret@uv.es

[b] Dr. D. Cangussu, Dr. Y. Journaux, R. Lescouëzec, Dr. E. Pardo
Institut Parisien de Chimie Moléculaire, UPMC-Univ. Paris 06
Paris, 75005 (France)
Fax:(+33)144273841
E-mail: emilio.pardo@uv.es
yves.journaux@upmc.fr

[c] Dr. Y. Journaux
UMR CNRS 7201, Institut Parisien de Chimie Moléculaire
Paris (France)

[d] Dr. J. Pasán, Prof. Dr. C. Ruiz-Pérez
Laboratorio de Rayos X y Materiales Moleculares
Departamento de Física Fundamental II, Universidad de La Laguna
La Laguna, 38201 Tenerife (Spain)

[e] Dr. E. Lhotel, Dr. C. Paulsen
CNRS, Institut Néel, BP166, Grenoble (France)

Supporting information for this article is available on the WWW under http://dx.doi.org/10.1002/chem.201101459.

of fundamental importance to high-density storage materials and molecular electronics.[6]

Among the molecule-based magnetic materials, the so-called single-chain magnets (SCMs),[7–14] which exhibit a slow relaxation of magnetisation below a blocking temperature (T_B), are particularly appealing to obtain M_4. Although Glauber[15] predicted in 1963 that a single chain with Ising-type magnetic anisotropy, either ferro- or ferrimagnetic, should present an exponential divergence of the relaxation time (τ) of the magnetisation as the temperature decreases, slow relaxation of the magnetisation in magnetically isolated chains was not observed until 2001.[8a] These compounds are called single-chain magnets (SCMs) by analogy with the so-called single-molecule magnets (SMMs).[16] These molecules have large ground-spin states (S) and negative axial magnetic anisotropies (D), which result in a high activation energy (E_a) for the magnetisation reversal, given by $E_a = |D|S^2$. In the case of SCMs, the activation energy also depends upon the intrachain magnetic coupling (J), given by the expression $E_a = (4|J| + |D|)S^2$.[16e] The main advantage of SCMs over SMMs is the theoretically increased possibility of achieving information storage at high temperatures. After the publication of the first example reported by Gatteschi and co-workers,[8a] which still exhibits the highest blocking temperature observed so far ($T_B \approx 15$ K),[8a] some additional examples of SCMs have been published over the last decade because of the possibility of storing information on these low-dimensional magnetic materials (1D).

However, from the relatively wide variety of examples of SCMs[7–14] published so far, none have shown other physical properties in addition to the magnetic ones. The combination of a slow relaxation of the magnetisation effects (characteristic of SCMs) and optical properties could supply new and exciting possibilities for storing information in the domain of M_4.

Herein, we present a rational enantioselective synthetic strategy for the synthesis of chiral heterobimetallic chains. The strategy is based on the use of enantiopure chiral sterically-hindered dianionic oxamatocopper(II) complexes with

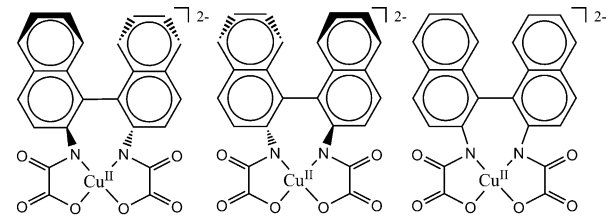

[(*M*)-Cu(*M*)-binaba]$^{2-}$ (**1**) [(*P*)-Cu(*P*)-binaba]$^{2-}$ (**2**) [Cu(binaba)]$^{2-}$ (**3**)

the enantiomerically pure (*M*)-1,1′-binaphthalene-2,2′-bis-(oxamate) [(*M*)-binaba] and (*P*)-1,1′-binaphthalene-2,2′-bis-(oxamate) [(*P*)-binaba] ligands These act as bis-bidentate ligands towards fully solvated, divalent transition-metal cations like manganese(II) and cobalt(II). These enantiopure copper(II) precursors transfer their chiral information to the stereochemistries of the M^{II} metal centres in a controlled manner. Therefore, this molecular-designed approach allows enantiopure oxamato-bridged heterobimetallic chains with four possible structures to be obtained (Scheme 1). Indeed, enantiopure chiral chains made by the repetition of the corresponding neutral chiral (*M*)-Cu^{II}-(Λ)-M^{II} (Scheme 1a) and (*P*)-Cu^{II}-(Δ)-M^{II} (Scheme 1b) units are obtained when using the mononuclear (*M*)- (**1**) and (*P*)-copper(II)-binaba (**2**) complexes, respectively. In contrast, when using the racemic mononuclear copper(II)–binaba complex (**3**) with manganese(II) or cobalt (II) ions, an achiral zigzag Cu^{II}M^{II} chain structure is obtained that consists of alternating [(*M*)-Cu^{II}-(Λ)-M^{II}]$_n$ and [(*P*)-Cu^{II}-(Δ)-M^{II}]$_n$ chains (Scheme 1a+b) instead of the more usual *meso* form (Scheme 1c). In a previous communication,[11c] we showed that the combination of an orbitally degenerate six-coordinate high-spin Co^{II} ion ($^4T_{1g}$) and a square-planar Cu^{II} precursor with bulky aromatically substituted oxamate ligands results in a large intrachain Ising-type magnetic anisotropy and a minimisation of the interchain interactions. Both conditions were necessary to observe the phenomenon of slow relaxation of the magnetisation in the cobalt(II)–copper(II) chain [CoCu(L^1)-(DMF)$_2$]·DMF (**1b**) in which the magnetic coupling between the Co^{II} and Cu^{II} ions through the oxamate bridge is large enough to allow a long-range intrachain magnetic correla-

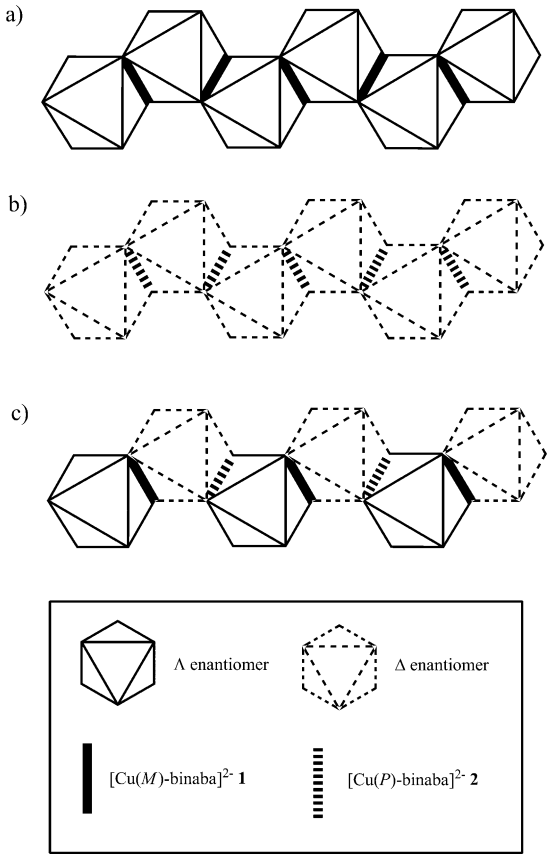

Scheme 1. Proposed structures of the enantiopure oxamato-bridged heterobimetallic chain compounds: a) [(*M*)-Cu^{II}-(Λ)-Mn^{II}]$_n$, b) (*P*)-Cu^{II}-(Δ)-Mn^{II}]$_n$ and c) meso-[(*M*)-Cu^{II}-(Λ)-Mn^{II}-(*P*)-Cu^{II}-(Δ)-Mn^{II}]$_n$.

tion ($J=-28.9\ cm^{-1}$). Moreover, chirality was induced in the corresponding heterobimetallic chain compound in a rational way, giving rise to the first example of an enantiopure, chiral single-chain magnet.

Herein, we report the preparation and structural and magnetic characterisation of a novel series of heterobimetallic chains of general formula $[MCuL^x(S)_m(H_2O)_n]\cdot aS\cdot bH_2O$ {**1a**: $L^x=L^1$, M=Mn, S=DMSO ($m=3$, $n=0$, $a=0.5$ and $b=3$); **1b**: $L^x=L^1$, M=Co, S=DMF ($m=2$, $n=0$, $a=1$ and $b=0$); **2a**: $L^x=L^2$, M=Mn, S=DMSO ($m=3$, $n=0$, $a=0.5$ and $b=3$); **2b**: $L^x=L^2$, M=Co, S=DMF ($m=2$, $n=0$, $a=1$ and $b=0$); **3a**: $L^x=L^3$, M=Mn, S=DMSO ($m=2$, $n=1$, $a=1$ and $b=1$); **3b**: $L^x=L^3$, M=Co, S=DMF ($m=2$, $n=0$, $a=2$ and $b=0$); L^1= [(*M*)-binaba], L^2= [(*P*)-binaba] and L^3=1,1′-binaphthalene-2,2′-bis(oxamate) (binaba)}. This work is thus the first example of a successful rational design of a new family of enantiopure oxamato-bridged heterobimetallic SCMs and their synthesis not only expands the range of reported examples of slow magnetically relaxing 1D materials, but it also introduces this hot topic into the exciting area of multifunctional materials.

Results and Discussion

Synthesis and general physical characterisation: The neutral oxamato-bridged $M^{II}Cu^{II}$ chains (M=Mn and Co) were synthesised in three successive steps (Scheme 2). The first step involves the synthesis of the *N*-substituted mono-oxamate ligands by straightforward condensation of ethyl chlorooxoacetate (2 equiv) with the corresponding enantiomeric or racemic mixture of 1,1′-binaphthyl-2,2′-diamine in THF (Scheme 2a). The ligands were isolated as the ethyl ester derivatives $H_2Et_2L^x$ ($x=1$–3) in very high yields (ca. 90–100%). The second step consists of the synthesis of the mononuclear copper(II)–L^x complexes as their tetrabutylammonium (nBu_4N) salts of general formula $[(TBA)_2Cu(L^x)]\cdot nH_2O$. These complexes were obtained (yield: 85–95%) by deprotonation and hydrolysis of the corresponding $HEtL^x$ ligand with nBu_4NOH in water and subsequent addition of a stoichiometric amount of $Cu(NO_3)_2\cdot 3H_2O$ (Scheme 2b). In the third step, the corresponding heterobimetallic chain compounds of general formula $[MCuL^x(S)_m(H_2O)_n]\cdot aS\cdot bH_2O$ were obtained by reaction of the corresponding tetrabutylammonium salt of the mononuclear Cu^{II} precursor and the nitrate salt of Mn^{II} in hot DMSO (**1a**–**3a**; Scheme 2c) or by slow diffusion in DMF in H-shaped tubes of solutions containing stoichiometric amounts of $[(nBu_4N)_2Cu(L^x)_2]\cdot nH_2O$ in one arm and of $Co(NO_3)_2\cdot 6H_2O$ in the other arm (**1b**–**3b**; Scheme 2c′). Up to now, our attempts to grow X-ray quality single crystals of the cobalt(II)–copper(II)–L^3 racemic chain analogue (**3b**) have been unsuccessful.

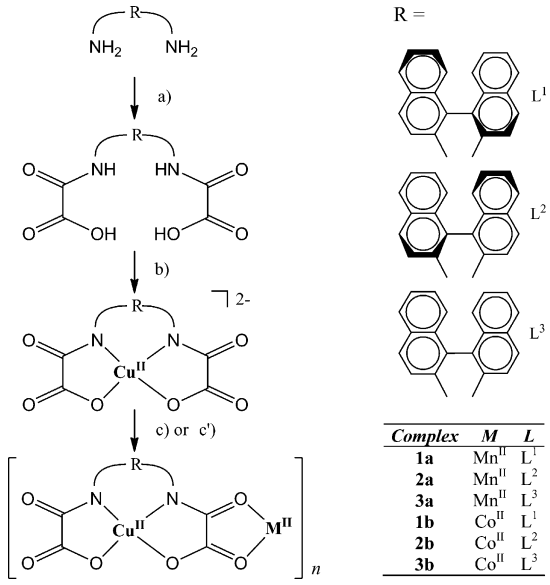

Complex	M	L
1a	Mn^{II}	L^1
2a	Mn^{II}	L^2
3a	Mn^{II}	L^3
1b	Co^{II}	L^1
2b	Co^{II}	L^2
3b	Co^{II}	L^3

Scheme 2. Synthetic pathway for the oxamato-bridged heterobimetallic chain compounds. Reagents and conditions: a) C_2O_2ClOEt, THF, 70°C; b) $NaOH/Cu^{II}(NO_3)_2\cdot 3H_2O$, H_2O, RT; c) $M^{II}(NO_3)_2\cdot 6H_2O/4H_2O$ (M=Co, Mn), DMSO, 60°C; c′) $Co^{II}(NO_3)_2\cdot 6H_2O$, DMF, RT.

The chemical identities of the ligands, the mononuclear copper(II) complexes and the chain compounds were confirmed by elemental analysis (C, H, Co, Cu, Mn and N) and IR and ^1H NMR spectroscopy. Analytical and selected spectroscopic data are listed in Tables S1 and S2 in the Supporting Information.

Description of the structures

*$[Cu\{(M)\text{-binaba}\}Mn(DMSO)_3]\cdot 0.5DMSO\cdot 3H_2O$ (**1a**), $[Cu\{(P)\text{-binaba}\}Mn(DMSO)_3]\cdot 0.5DMSO\cdot 3H_2O$ (**2a**) and $[Cu(binaba)Mn(H_2O)(DMSO)_2]\cdot DMSO\cdot H_2O$ (**3a**)*: The crystal structures of complexes **1a**, **2a** and **3a** were solved by single-crystal X-ray diffraction by using synchrotron radiation of the BM16 beamline at the ESRF (**1a**) and graphite-monochromated $Mo_{K\alpha}$ radiation with a Nonius–KappaCCD diffractometer (**2a** and **3a**). Complexes **1a** and **2a** crystallise in the non-centrosymmetric $P2_12_12_1$ space group and their absolute configurations could be reliably assigned (Table 1) whereas compound **3a** crystallises in the centrosymetric $P2_1/c$ space group. Their structures consist of enantiomerically pure (**1a** and **2a**) and achiral (**3a**) oxamato-bridged $Cu^{II}Mn^{II}$ chains and coordinated and crystallisation DMSO and H_2O molecules (Figures 1 and S1 in the Supporting Information).

The bis(oxamato)copper(II) entity acts as a bis-bidentate ligand through the *cis* carbonyl oxygen atoms towards *cis*-bis(dimethyl sulfoxide)manganese(II) units. This situation contrasts with that found for other reported heterobimetallic oxamato-bridged chains[17b] in which *trans* coordination of the two solvent molecules at the manganese(II) ions leads to linear chain structures. Selected bond lengths and angles for **1a**–**3a** are reported in Table 2. The copper environment is a severely distorted square-based pyramid with two amide nitrogen atoms [Cu–N=1.931(7)–1.939(6) Å for **1a**, Cu–N=1.940(8)–1.951(6) Å for **2a** and Cu–N=1.951(4)–1.957(4) Å for **3a**] and two carboxylate oxygen atoms [Cu–O=1.993(6)–2.003(6) Å for **1a**, Cu–O=1.993(6)–1.999(6) Å

Table 1. Summary of crystallographic data for **1a**–**3a**, **1b** and **2b**.

	1a	**2a**	**3a**	**1b**	**2b**
formula	$C_{31}H_{39}CuMnN_2O_{12.5}S_{3.5}$	$C_{31}H_{39}CuMnN_2O_{12.5}S_{3.5}$	$C_{30}H_{34}CuMnN_2O_{11}S_3$	$C_{33}H_{33}CoCuN_5O_9$	$C_{33}H_{33}CoCuN_5O_9$
M	870.40	870.40	813.22	766.11	766.11
crystal system	orthorhombic	orthorhombic	monoclinic	orthorhombic	orthorhombic
space group	$P2_12_12_1$	$P2_12_12_1$	$P2_1/c$	$C222_1$	$C222_1$
a [Å]	8.8660(18)	8.8568(2)	8.8231(2)	10.566(2)	10.730(2)
b [Å]	18.597(4)	18.7469(5)	18.7744(4)	15.364(3)	15.738(3)
c [Å]	28.241(6)	28.2809(7)	20.9707(6)	19.755(4)	19.675(4)
β [°]	–	–	98.7230(10)	–	–
V [Å^3]	4656.4(16)	4695.7(2)	3433.58(15)	3207.0(11)	3322.5(11)
Z	4	4	4	4	4
D_{calcd} [g cm^{-3}]	1.277	1.228	1.565	1.587	1.532
$F(000)$	1848	1792	1656	1576	1576
T [K]	100(2)	293(2)	293(2)	293(2)	293(2)
$\mu(Mo_{K\alpha})$ [mm^{-1}]	0.959	0.928	1.230	1.384	1.326
unique reflections	7408	9626	6770	3645	3923
reflections with $I>2\sigma(I)$	6787	7903	5040	3607	3775
Flack parameter	0.01(3)	0.09(4)	–	−0.037(17)	−0.011(18)
R_1[a] [$I>2\sigma(I)$] (all)	0.0980 (0.1033)	0.1068 (0.1270)	0.0634 (0.0963)	0.0473 (0.0476)	0.0454 (0.0469)
wR_2[b] [$I>2\sigma(I)$] (all)	0.2815 (0.2910)	0.2933 (0.3107)	0.1472 (0.1700)	0.1299 (0.1304)	0.1243 (0.1269)
S[c]	1.341	1.144	1.151	1.061	1.053

[a] $R_1=\Sigma(|F_o|-|F_c|)/\Sigma|F_o|$. [b] $wR_2=[\Sigma w(F_o^2-F_c^2)^2/\Sigma w(F_o^2)^2]^{1/2}$. [c] $S=[\Sigma w(|F_o|-|F_c|)^2/(N_o-N_p)]^{1/2}$.

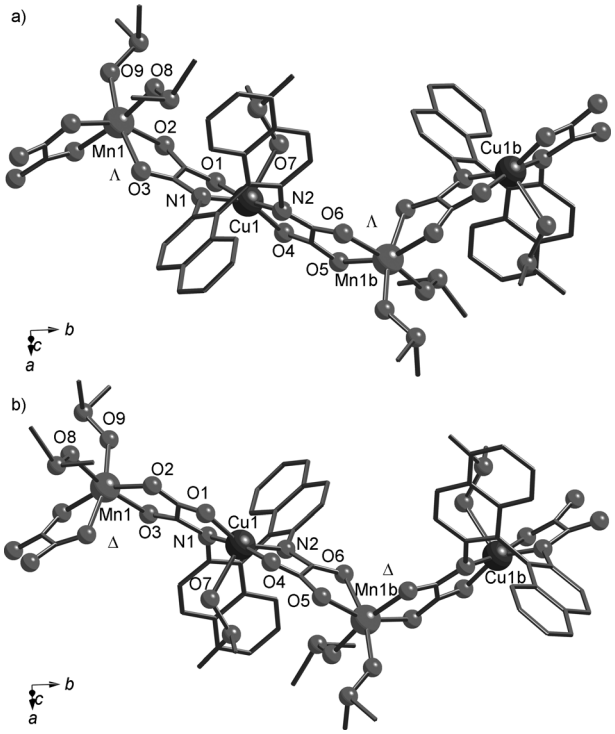

Figure 1. Images of fragments of the chains of a) **1a** and b) **1b** with atom labelling of the metal coordination environments. Hydrogen atoms have been omitted for clarity (symmetry codes for **1a**: $b=-x+1$, $y+{}^1/_2$, $-z+{}^3/_2$; for **1b**: $b=-x+1$, $y-{}^1/_2$, $-z+{}^1/_2$).

for **2a** and Cu−O = 1.980(3)–1.983(3) Å for **3a**] in the basal plane and a weakly coordinated DMSO molecule in the apical position [Cu1−O7 = 2.279(6) Å for **1a**, Cu1−O7 = 2.297(8) for **2a** and Cu1−O7 = 2.397(4) for **3a**; Table 2]. The large deviations from the CuN_2O_2 mean plane [0.568(6) Å for N1 and 0.435(5) Å for O1 in **1a**, 0.607(7) Å for N2 and 0.405(6) Å for O1 in **2a** and 0.602(4) Å for N2 and 0.365(3) Å for O1 in **3a**] result in a remarkable tetrahedral distortion of the basal plane of Cu1 [dihedral angles between the N1-Cu1-O1 and N2-Cu1-O4 planes of 33.6(2), 33.4(2) and 32.50(12)° for **1a**, **2a** and **3a**, respectively], with only one of the two possible enantiomers (*M* and *P* for **1a** and **2a**, respectively) being present, and regular alternation of the two enantiomers (*M* and *P*) in neighbouring chains in **3a**.

The manganese atom is six-coordinate with four carbonyl oxygen atoms from two oxamate ligands and two DMSO molecules (**1a** and **2a**) or one DMSO and one water molecule (**3a**) in a *cis* disposition giving a distorted octahedral environment [Mn−O = 2.109(7)–2.209(6) Å for **1a**, Mn−O = 2.139(8)–2.215(6) Å for **2a** and Mn−O = 2.148(3)–2.211(3) Å for **3a**; Table 2]. Only the Λ isomer is present in **1a** while **2a** contains only the Δ isomer. The repetition of (*M*)-Cu^{II}-(Λ)-Mn^{II} (**1a**) and (*P*)-Cu^{II}-(Δ)-Mn^{II} (**2a**) chiral units leads to the formation of enantiopure chiral wave-like chain structures (Figure 2a and b). In contrast, in **3a**, two different types of chain alternate regularly in the crystal lattice, that is, it consists of the repetition of (*M*)-Cu^{II}-(Λ)-Mn^{II} and (*P*)-Cu^{II}-(Δ)-Mn^{II} motifs, which leads to an achiral wave-like chain structure. The coordination sphere and bond lengths around the manganese(II) ions in all three chain compounds are similar to those observed in the related oxamato-bridged manganese(II)–copper(II) chain $[MnCu(opba)_2(DMSO)_3]$ [opba = *ortho*-phenylenebis(oxamate)].[17c] The intrachain Mn1···Cu1 distances through the oxamato bridge [5.347(2)–5.399(2) Å for **1a**, 5.359(2)–5.411(2) Å for **2a** and 5.3662(8)–5.4171(8) Å for **3a**] compare well with those reported for $[MnCu(opba)_2(DMSO)_3]$ [5.394(1)–5.442(1) Å].

The chains of **1a**–**3a** running in the [010] direction of the crystal lattice are well separated from each other (Figure S2). The bulky aromatic rings of the ligands, as well as

Table 2. Selected bond lengths [Å] and angles [°] in **1a**–**3a**.[a,b]

	1a	**2a**	**3a**
Cu1−N1	1.931(7)	1.940(8)	1.951(4)
Cu1−N2	1.939(6)	1.951(6)	1.957(4)
Cu1−O1	1.993(5)	1.993(6)	1.980(3)
Cu1−O4	2.003(6)	1.999(6)	1.983(3)
Cu1−O7	2.279(6)	2.297(8)	2.397(4)
Mn1−O2	2.209(6)	2.197(7)	2.199(3)
Mn1−O3	2.157(6)	2.177(6)	2.179(3)
Mn1−O5a	2.203(7)	2.192(7)	2.211(3)
Mn1−O6a	2.111(6)	2.215(6)	2.211(3)
Mn1−O8	2.172(6)	2.186(7)	2.192(4)
Mn1−O9	2.109(7)	2.139(8)	–
Mn1−O1w	–	–	2.148(3)
O1-Cu1-O4	98.8(2)	99.2(3)	98.44(13)
O1-Cu1-O7	97.6(2)	97.2(3)	100.25(15)
O4-Cu1-O7	83.9(3)	84.8(3)	82.87(15)
N1-Cu1-O1	84.1(2)	84.1(3)	84.35(13)
N1-Cu1-O4	170.2(3)	170.6(3)	170.23(15)
N1-Cu1-O7	86.4(3)	86.1(3)	87.43(15)
N2-Cu1-O1	149.1(2)	149.2(3)	150.31(15)
N2-Cu1-O4	84.3(3)	83.7(3)	83.69(14)
N2-Cu1-O7	113.2(3)	113.6(3)	109.38(16)
N2-Cu1-N1	98.1(3)	98.0(3)	98.56(15)
O3-Mn1-O2	75.9(2)	75.8(2)	75.89(11)
O5-Mn1-O2	157.5(2)	156.6(3)	157.62(12)
O5a-Mn1-O3	93.9(2)	93.5(2)	93.56(12)
O6a-Mn1-O2	86.1(2)	85.6(2)	87.30(11)
O6a-Mn1-O3	98.2(2)	99.4(2)	102.25(12)
O6a-Mn1-O5	75.4(2)	75.6(3)	75.55(12)
O6a-Mn1-O8	84.9(2)	84.7(3)	86.47(15)
O8-Mn1-O2	94.0(2)	94.9(3)	93.06(13)
O8-Mn1-O3	169.2(2)	169.4(3)	165.40(15)
O8-Mn1-O5a	96.8(2)	97.0(3)	100.00(15)
O9-Mn1-O2	104.4(3)	106.3(3)	–
O1w-Mn1-O2	–	–	109.34(13)
O9-Mn1-O3	91.9(3)	91.1(3)	–
O1w-Mn1-O3	–	–	93.02(13)
O9-Mn1-O5a	95.8(3)	94.5(3)	–
O1w-Mn1-O5a	–	–	90.62(13)
O9-Mn1-O6a	166.9(2)	165.9(3)	–
O1w-Mn1-O6a	–	–	159.86(13)
O9-Mn1-O8	86.7(3)	86.6(3)	–
O1w-Mn1-O8	–	–	81.52(15)

[a] The estimated standard deviations are given in parentheses. [b] Symmetry codes for **1a**: $a=-x+1$, $y-{}^1/_2$, $-z+{}^3/_2$; for **2a** and **3a**: $a=-x+1$, $y+{}^1/_2$, $-z+{}^1/_2$.

the coordinated DMSO molecules, afford effective shielding of the metal ions of the neighbouring chains, the shortest interchain metal–metal distances being as follows: Mn1···Mn1 = 8.866(2) Å and Mn1···Cu1 = 8.042(2) Å for **1a**, Mn1···Mn1 = 8.857(2) Å and Mn1···Cu1 = 8.0979(17) Å for **2a** and Mn1···Mn1 = 7.8324(9) Å and Mn1···Cu1 = 8.0587(9) Å for **3a**. Interestingly, the shortest interchain Mn···Mn distance is shorter (ca. 1 Å) for the racemic chain compound **3a** than for the enantiopure compounds **1a** and **2a** because of the regular alternation of (*M*)-(Λ) and (*P*)-(Δ) motifs in **3a**, which allows an effective approach of two neighbouring chains (Figures 2 and S2 in the Supporting Information).

*[Cu{(M)-binaba}Co(DMF)$_2$]·DMF (**1b**) and [Cu{(P)-binaba}Co(DMF)$_2$]·DMF (**2b**)*: Compounds **1b** and **2b** crystallise in the non-centrosymmetric $C222_1$ space group and their absolute configurations could be reliably assigned. Their structures consist of enantiomerically pure, oxamato-bridged $Cu^{II}Co^{II}$ chains and both coordinated and crystallisation DMF molecules (Figure 3). Within each chain, the bis(oxamato)copper(II) entity acts as a bis-bidentate ligand through the *cis* carbonyl oxygen atoms towards the *cis*-bis(dimethylformamide)cobalt(II) units. This situation contrasts with that found for other reported heterobimetallic oxamato-bridged chains with the formula [CoCu(Me$_3$pma)$_2$(H$_2$O)$_2$]·4H$_2$O [Me$_3$pma = *N*-2,4,6-trimethylphenyl(oxamate)][11a] in which the *trans* coordination of two water molecules to the cobalt atoms leads to a linear chain structure. Selected bond lengths and angles for **1b** and **2b** are reported in Table 3.

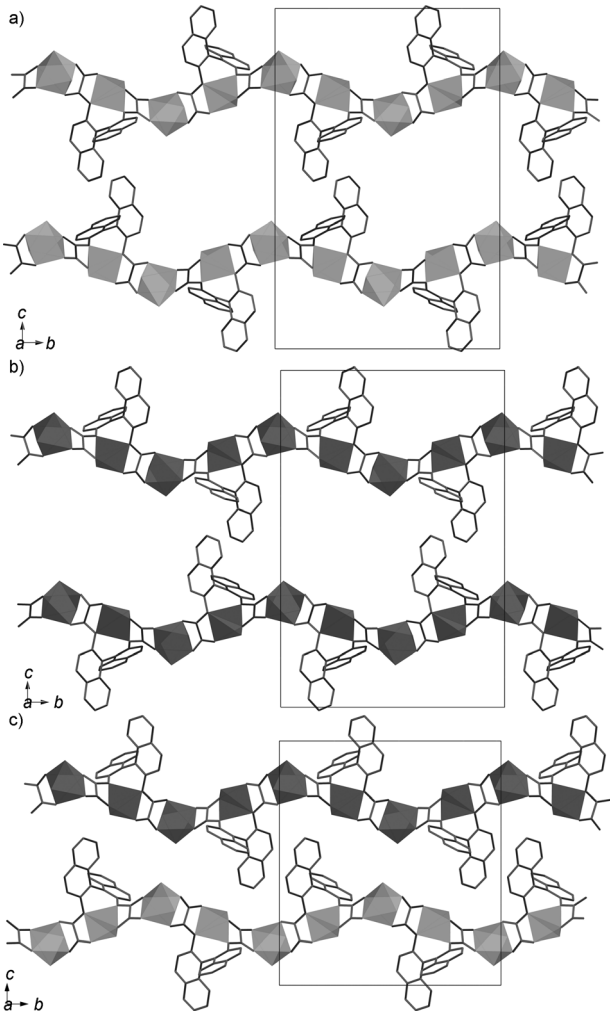

Figure 2. Images of the crystal packing of chains of a) **1a**, b) **2a** and c) **3a** in the *bc* plane. Hydrogen atoms and crystallisation solvent molecules have been omitted for clarity. The (Λ)-Mn^{II} and (Δ)-Mn^{II} atoms are depicted as light and dark octahedral polyhedra, respectively. The light and dark square-based pyramidal polyhedra represent the (*M*)-Cu^{II} and (*P*)-Cu^{II} atoms, respectively.

The copper atoms are four-coordinate with two amidate nitrogen and two carboxylate oxygen atoms from the two oxamate groups, giving a severely distorted square-planar

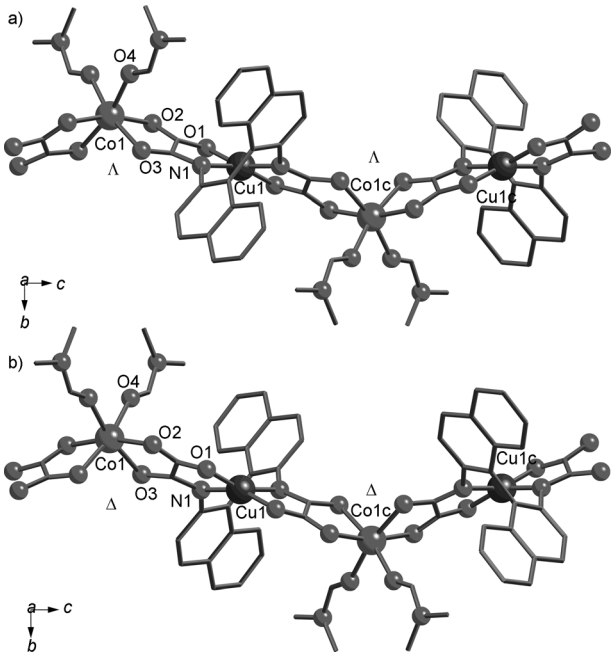

Figure 3. Images of fragments of the chains of a) **1b** and b) **2b** with the atom labelling of the metal coordination environments. Hydrogen atoms have been omitted for clarity (symmetry code: $c=-x+1, -y, z+1/2$).

Table 3. Selected bond lengths [Å] and angles [°] in **1b** and **2b**.[a,b]

	1b	**2b**
Cu1–N1	1.952(2)	1.941(2)
Cu1–O1	1.960(2)	1.956(2)
Co1–O2	2.100(2)	2.100(2)
Co1–O3	2.119(2)	2.108(2)
Co1–O4	2.091(3)	2.079(2)
O1-Cu1-O1a	97.68(13)	100.18(13)
O1-Cu1-N1	85.33(9)	84.87(9)
O1-Cu1-N1a	158.65(9)	157.28(11)
N1-Cu1-N1a	99.56(13)	99.05(3)
O2-Co1-O2b	164.79(12)	166.29(14)
O2-Co1-O3	79.90(8)	79.51(9)
O2-Co1-O3b	90.51(8)	91.70(9)
O2-Co1-O4	100.18(9)	91.86(11)
O2-Co1-O4b	91.19(10)	98.27(11)
O3-Co1-O4	88.01(10)	167.85(12)
O3-Co1-O4b	166.47(10)	87.98(13)
O3-Co1-O3b	102.12(13)	100.71(15)
O4-Co1-O4b	83.54(17)	84.8(2)

[a] The estimated standard deviations are given in parentheses. [b] Symmetry codes: $a=x, -y, -z+1$; $b=-x+1, y, -z+1/2$.

environment [Cu1–N1 = 1.952(2) Å and Cu1–O1 = 1.960(2) Å for **1b** and Cu–N1 = 1.941(2) Å and Cu–O1 = 1.956(2) Å for **2b**]. The large deviations from the CuN_2O_2 mean plane of 0.384(3) Å for N1 and 0.340(2) Å for O1 in **1b** and 0.387(3) Å for N1 and 0.380(3) Å for O1 in **2b** result in a remarkable tetrahedral distortion of the Cu1 environment [dihedral angles between the N1-Cu1-O1 and N1a-Cu1-O1a planes of 31.69(9) and 33.93(9) for **1b** and **2b**, respectively], with only one of the two possible enantiomers *M* and *P* for **1b** and **2b**, respectively, being present. The cobalt atom is six-coordinate with two DMF molecules in a *cis* disposition and four carbonyl oxygen atoms from two oxamate ligands leading to a distorted octahedral environment [Co–O = 2.091(3)–2.119(2) Å for **1b** and Co–O = 2.079(2)–2.108(2) Å for **2b**]. In contrast to the situation found in the related achiral, oxamato-bridged cobalt(II)–copper(II) zigzag chain $[CoCu(Me_3pma)_2(H_2O)_2]\cdot 4H_2O$,[11a] only one isomer, the Λ in **1b** and the Δ in **2b**, is present, which confirms the transmission of chiral properties from the enantiopure ligand precursor to the corresponding heterobimetallic chain compound. The repeating of the neutral chiral (*M*)-Cu^{II}-(Λ)-Co^{II} (**1b**) and (*P*)-Cu^{II}-(Δ)-Co^{II} (**2b**) motifs leads to the formation of enantiopure chiral wave-like chain structures (Figure 4). The coordination spheres and bond lengths around the cobalt atoms in both chain compounds are similar to those observed for the high-spin Co^{II} ion in the related oxamato-bridged cobalt(II)–copper(II) chains in [CoCu-

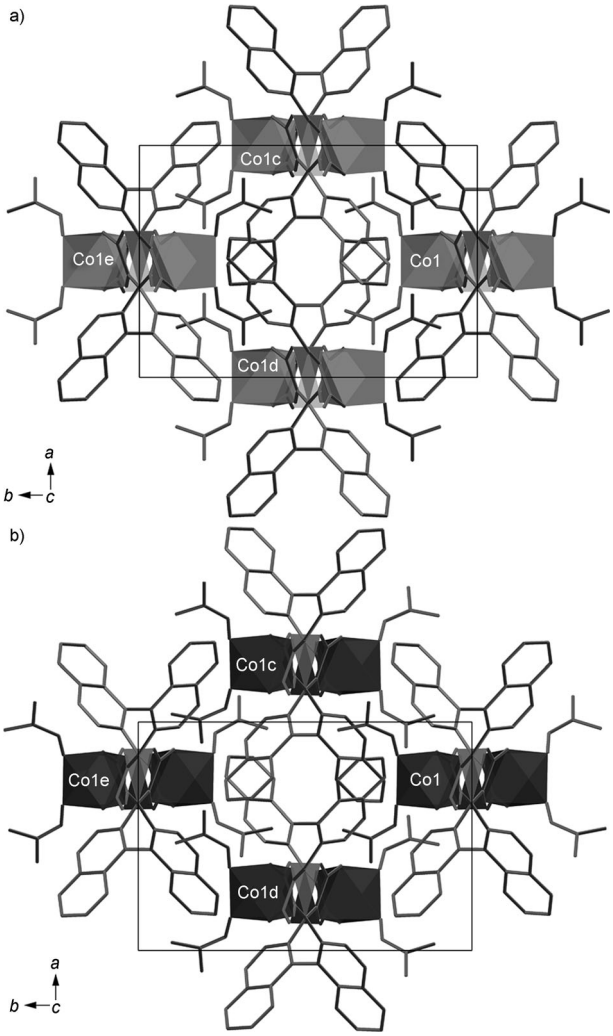

Figure 4. Crystal packing of the chains of a) **1b** and b) **2b** along the [001] direction. The (Λ)-Co^{II} and (Δ)-Co^{II} atoms are depicted as light and dark octahedral polyhedra, respectively. The light and dark tetrahedral polyhedra represent the (*M*)-Cu^{II} and (*P*)-Cu^{II} atoms, respectively. Hydrogen atoms and crystallisation dimethylformamide molecules have been omitted for clarity (symmetry codes: $c=x+1/2, y+1/2$; $d=x-1/2, y+1/2, z$; $e=x, y+1, z$).

$(Me_2pma)_2(H_2O)_2]$ [Me_2pma = *N*-(2,6-dimethylphenyl)oxamate].[11b] The intrachain Co1···Cu1 distances through the oxamato bridge are 5.298(1) Å for **1b** and 5.292(1) Å for **2b**, which compare well with that reported for [CoCu$(Me_2pma)_2(H_2O)_2$] [Co···Cu = 5.298(1) Å].

The chains of **1b** and **2b** follow a 2_1 screw axis that runs parallel to the [001] direction and they are even more separated from each other than in the case of the $Mn^{II}Cu^{II}$ chain compounds **1a**–**3a** (Figure S3 in the Supporting Information). The bulky aromatic rings of the ligands afford effective shielding between the metal ions of neighbouring chains, the shortest interchain Co1···Co1 and Co1···Cu1 distances being 9.3233(15) and 9.1947(12) Å, respectively, for **1b** and 9.5239(15) and 9.2827(11) Å, respectively, for **2b**.

Optical properties: The circular dichroism (CD) spectra of the pro-ligands H_2Et_2-(*M*)-binaba ($H_2Et_2L^1$) and H_2Et_2-(*P*)-binaba ($H_2Et_2L^2$), the copper(II) precursors $(nBu_4N)_2\{[Cu(L^1)]\}\cdot 2H_2O$ (**1**) and $(nBu_4N)_2\{[Cu(L^2)]\}\cdot 2H_2O$ (**2**) and the enantiopure $Mn^{II}Cu^{II}$ chains **1a** and **2a** and the $Co^{II}Cu^{II}$ chain compounds **1b** and **2b** were recorded to confirm their chirality and enantiomerically pure nature. Figure 5a shows the CD spectra of the two enantiomers of the pro-ligands $H_2Et_2L^1$ and $H_2Et_2L^2$ and the copper(II) precursors **1** and **2** recorded in acetonitrile; it can be seen that the spectra of the pairs of enantiomers are almost mirror images of each other. In the case of **1**, the spectra exhibit maximum positive Cotton effects at 210 and 370 nm and maximum negative effects are observed at 230, 250, 275 and 628 nm. The bands in the UV region can be assigned to metal-to-ligand (ML) charge-transfer and intraligand (IL) transitions. The bands in the CD spectra of **1** and **2** in the visible region, which do not appear in the CD spectra of the ligands (see inset in Figure 5a), can be attributed to d–d transitions as a result of a chirality-induced effect on the copper(II) ions by the corresponding (*M* or *P*) enantiopure ligand.

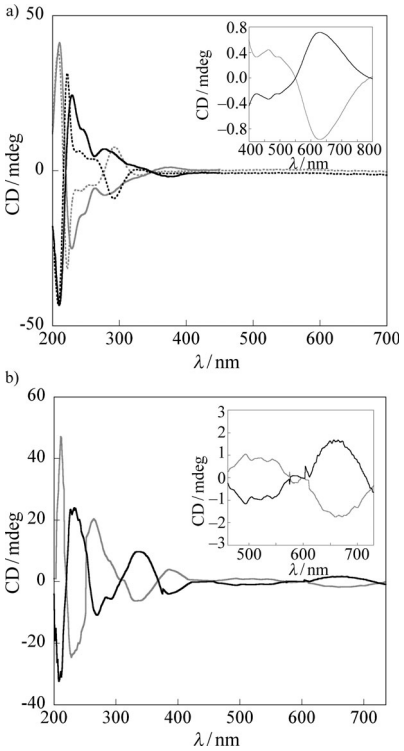

Figure 5. a) CD spectra of **1** (——), **2** (——), H_2Et_2-(*M*)-binaba (•••••) and H_2Et_2-(*P*)-binaba (•••••) in CH_3CN (10^{-5} mol L^{-1}). The inset shows the CD spectra of **1** (——) and **2** (——) in the visible region. b) CD spectra of **1b** (——) and **2b** (——) as KBr pellets (1 mg in 100 mg of KBr). The inset shows the CD spectra in the visible region. mdeg = millidegree.

The solid CD spectra of the heterobimetallic chain compounds **1a** and **2a** and **1b** and **2b**, shown in Figures S4 and 5b, respectively, confirm the absolute configurations of the chiral metal centres. The CD spectra show an almost mirror image of the corresponding enantiomer. They exhibit maximum positive Cotton effects at 215, 265 and 400 nm (**1a**) and 210, 270 and 400 nm (**1b**), and maximum negative effects at 230 and 335 nm (**1a**) and 235 and 350 nm (**1b**). They are the result of a chirality-induced effect on the two metal centres by the enantiopure ligand. The bands in the visible region of the CD spectra of **1a**, **2a**, **1b** and **2b** can be attributed to d–d transitions, whereas those in the UV region have been assigned to metal-to-ligand (ML) charge-transfer and intraligand (IL) transitions by comparison with the solution CD spectra of the pro-ligands and copper(II) precursors (Figure 5a).

Static magnetic properties

Manganese(II)–copper(II) chains: The direct current (dc) magnetic properties of **1a**–**3a** in the form of a $\chi_M T$ versus T plot, χ_M being the magnetic susceptibility per MnCu pair, are shown in Figure 6a. At room temperature, the values of $\chi_M T$ vary in the narrow range 4.21–4.36 $cm^3 mol^{-1} K$, which is smaller than expected for the sum of a square-planar Cu^{II} ion [$S_{Cu} = {}^1/_2$, $\chi_M T = (N\beta^2 g_{Cu}{}^2/3k) S_{Cu}(S_{Cu}+1) =$ 0.40 $cm^3 mol^{-1} K$, with $g_{Cu} = 2.1$] and an octahedral high-spin Mn^{II} ion [$S_{Mn} = {}^5/_2$, $\chi_M T = (N\beta^2 g_{Mn}{}^2/3k) S_{Mn}(S_{Mn}+1) =$ 4.37 $cm^3 mol^{-1} K$, with $g_{Mn} = 2.0$] magnetically isolated, suggesting a relatively large intrachain antiferromagnetic interaction between the Cu^{II} and Mn^{II} ions through the oxamate bridge. Upon cooling, $\chi_M T$ decreases first and attains minima at 107, 110 and 79 K for **1a**, **2a** and **3a**, respectively (inset in Figure 6a). The presence of minima in the $\chi_M T$ versus T plots of **1a**–**3a** is a characteristic of ferrimagnetic manganese(II)–copper(II) chain compounds.[17] Finally, $\chi_M T$ increases to values of 74.7 and 58.4 $cm^3 mol^{-1} K$ at 2.0 K for **1a** and **2a**, respectively, under a dc magnetic field of 100 G. In the case of **3a**, $\chi_M T$ increases and reaches a maximum of 58.4 $cm^3 mol^{-1} K$ at around 5.0 K and then decreases, probably due to intermolecular interactions (see below).

The M versus H plots for **1a**, **2a** and **3a** at 2.0 K, M being the magnetisation per MnCu pair and H the applied magnetic field, are shown in Figure 6b. The magnetisation values at 5.0 T ($M = 3.90$–$3.94\ N\beta$) are consistent with those predicted for an $S = 2$ state resulting from antiferromagnetic coupling between a high-spin Mn^{II} centre ($S_{Mn} = {}^5/_2$, $g_{Mn} =$

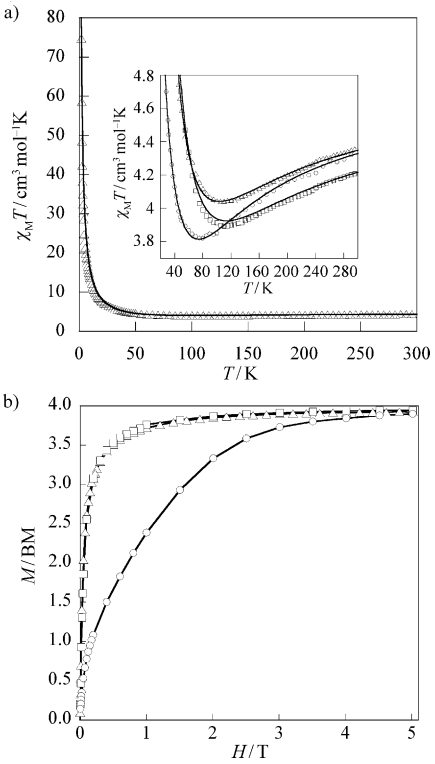

Figure 6. a) Temperature dependence of $\chi_M T$ of **1a** (△) under an applied magnetic field of 1 T ($T \geq 50$ K) and 100 G ($T < 50$ K). The inset shows the minima of $\chi_M T$ of **1a** (△), **2a** (□) and **3a** (○). The solid lines are the best-fit curves (see text). b) Field dependence of M for **1a** (△), **2a** (□) and **3a** (○) at 2.0 K. The solid lines are guides to the eye. BM = Bohr magneton.

2.0) and a Cu^{II} ion ($S_{Cu} = {}^1/_2$, $g_{Cu} = 2.1$) along the chain [$M_S = (g_{Mn}S_{Mn} - g_{Cu}S_{Cu})N\beta = 3.90N\beta$]. Interestingly, the magnetisation isotherms of **1a** and **2a** show a fast saturation with around 98% of the M_S value reached within a field of 1000 G. This reveals a strong short-range correlation along the chain favouring the antiparallel alignment of the spins of the Cu^{II} and Mn^{II} ions. However, there is a much slower increase in the magnetisation values with applied field for the racemic compound **3a** (Figure 6b). The shape of the M versus H plot for **3a**, in contrast to those observed for **1a** and **2a**, suggests weaker intramolecular magnetic coupling and/or antiferromagnetic interchain interactions. These interchain interactions would be present only to a significant extent in **3a**, in agreement with the shorter interchain distances in **3a** relative to those in **1a** and **2a**.

The magnetic susceptibility data of the manganese(II)–copper(II) chain compounds **1a–3a** were analysed by using the well-known one-dimensional model developed first by Seiden[18a] and later by Georges and Curély[18b,c] and their co-workers. In this model, the Mn^{II} and Cu^{II} ions are treated as classic ($S_{Mn} = {}^5/_2$) and quantum ($S_{Cu} = {}^1/_2$) spins, respectively, and the spin Hamiltonian is expressed by Equation (1), in which i extends over the MnCu units, J is the magnetic coupling parameter, g_{Mn} and g_{Cu} are the Landé factors of the Mn^{II} and Cu^{II} ions, β is the Bohr magnetón and H is the applied magnetic field.

$$\mathbf{H} = \sum\nolimits_i [-J\mathbf{S}_{Mn,i}(\mathbf{S}_{Cu,i}\mathbf{S}_{Cu,i-1}) + (g_{Mn}\mathbf{S}_{Mn,i} + g_{Cu}\mathbf{S}_{Cu,i})\beta H] \quad (1)$$

The least-squares fit of the experimental data by this model (by fixing the value of $g_{Mn} = 2.0$) in the temperature range 6–300 K gave values for $-J$ and g_{Cu} (Table 4). The theoretical curves reproduce quite well the observed minima of the $\chi_M T$ versus T plots (solid lines in the inset in Figure 6a). The antiferromagnetic coupling between the Cu^{II} and Mn^{II} ions through the oxamate bridge in **1a–3a** is somewhat weaker than that observed for the related chain [MnCu(opba)$(H_2O)_2$]·DMSO[17b] ($J = -32.1$ cm^{-1}). The reason for this lies in the tetrahedral distortion of the environment of the Cu^{II} atoms in **1a–3a** and in the subsequent large deviations from the CuN_2O_2 mean plane. The copper atom in the previously reported MnCu chain lies in the oxamato plane, which leads to a better overlap of the magnetic orbitals of the Cu^{II} and Mn^{II} ions through the σ in-plane exchange pathway of the oxamato bridge and thus to a stronger antiferromagnetic coupling. The observed values of the distances and angles around the copper(II) ion in **1a–3a** are very similar. Thus, the weaker J value found for **3a** when compared with the enantiopure compounds **1a** and **2a** can only be explained by paying attention to the coordination environment of the manganese atoms. A thorough inspection of the crystal structures of **1a–3a** showed no significant discrepancies in the Mn–O distances. However, some important differences are found by looking at the *cis* (α and β) and *trans* (γ) interbond angles (see Table 4). Although the values of α and β are almost identical for **1a–3a**, those of γ differ drastically between **1a**, **2a** and **3a** (Table 4). This relatively important distortion in the racemic compound **3a** would account for the weaker antiferromagnetic coupling found in this compound, as observed in similar systems.[19]

Table 4. Selected magneto-structural data for the $Mn^{II}Cu^{II}$ chain compounds.

Complex	$-J$ [cm^{-1}][a]	g_{Cu}[b]	α [°][c]	β [°][c]	γ [°][c]
1a	25.2	2.10	157.5(2)	166.9(2)	169.2(2)
2a	26.6	2.15	156.6(3)	165.9(3)	169.4(3)
3a	18.9	2.10	157.62(12)	165.40(15)	159.86(13)

[a] Intrachain magnetic coupling parameter. [b] Landé factor. [c] Interbond angles O2-Mn1-O5 (α), O6-Mn1-O9 (β) and O3-Mn1-O8 (γ).

Cobalt(II)–copper(II) chains: The dc magnetic properties of **1b–3b** presented in the form of the $\chi_M T$ versus T plot (χ_M being the molar magnetic susceptibility per CuCo pair and T the temperature) are shown in Figure 7a. At room temperature, the values of $\chi_M T$ (in the range 3.05–3.32 cm^{3}mol^{-1}K) are slightly below that expected for the sum of a square-planar Cu^{II} ion ($S_{Cu} = {}^1/_2$, $\chi_M T = 0.40$ cm^{3}mol^{-1}K, with $g = 2.1$) and an octahedral high-spin

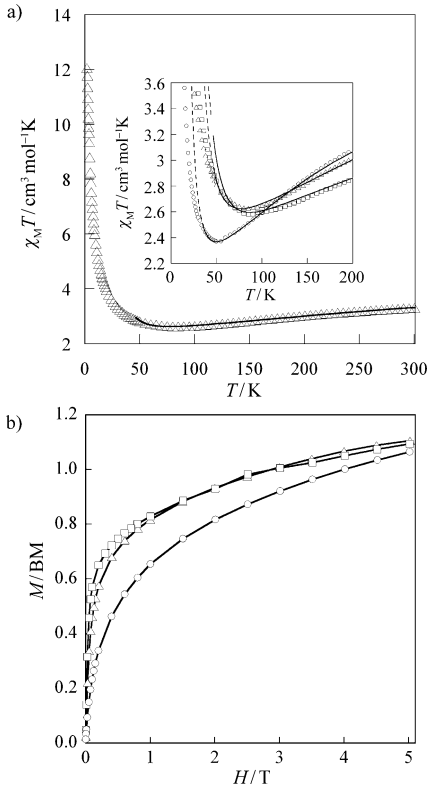

Figure 7. a) Temperature dependence of $\chi_M T$ of **1b** (△) under an applied magnetic field of 1 T ($T \geq 50$ K) and 250 G ($T < 50$ K). The inset shows the minima of $\chi_M T$ of **1b** (△) and **2b** (□) and **3b** (○). The solid lines are the best-fit curves (see text). b) Field dependence of M for **1b** (△) and **2b** (□) and **3b** (○) at 2.0 K. The solid lines are guides to the eye.

Co^{II} centre[20] ($S_{Co} = {}^3/_2$) with an orbitally degenerate $^4T_1$ single-ion ground state ($L_{Co} = 1$, $\chi_M T = 2.5$–3.0 cm^3 mol^{-1} K) magnetically isolated. Upon cooling, $\chi_M T$ decreases first and attains minima at 85, 85 and 51 K for **1b**, **2b** and **3b**, respectively (see inset in Figure 7a). This behaviour is typical of ferrimagnetic cobalt(II)–copper(II) chain compounds.[10] Finally, as T is further lowered, $\chi_M T$ increases to reach values of 12.1 (**1b**) and 18.0 cm^3 mol^{-1} K (**2b**) at 2.0 K under a dc magnetic field of 100 G. In the case of **3b**, $\chi_M T$ increases and reaches a maximum at around 5.0 K with a $\chi_M T$ value of 11.9 cm^3 mol^{-1} K owing to the magnetic anisotropy and/or antiferromagnetic interchain interactions. The lack of a maximum of χ_M allows us to rule out the occurrence of 3D long-range antiferromagnetic order,[21] the chains thus being magnetically well isolated.

The M versus H plots for **1b**–**3b** at 2.0 K (M being the magnetisation per CoCu pair) are shown in Figure 7b. The magnetisation values at 5.0 T ($M = 1.05$–$1.10\ N\beta$) are consistent with the value predicted for partial spin cancellation resulting from antiferromagnetic coupling between a high-spin Co^{II} ion ($S_{eff} = {}^1/_2$, $g = 4.2$)[20] and a Cu^{II} ion ($S = {}^1/_2$, $g = 2.1$, $M_s = 1.10\ N\beta$). Moreover, the magnetisation isotherms of **1b** and **2b** show fast saturation with around 80% of the M_S value reached within a field of 1000 G. This reveals a strong short-range correlation along the chain favouring the antiparallel alignment of the spins of the Cu^{II} and Co^{II} ions. As far as the racemic compound **3b** is concerned, similar to what occurred for the racemic CuMn chain **3a**, the increase in magnetisation with applied field (Figure 7b) is less than with the enantiopure CoCu chain compounds **1b** and **2b**. Thus, we conclude that weaker intramolecular magnetic coupling and/or antiferromagnetic interchain interactions are involved in **3b**.

To analyse the magnetic susceptibility data of the cobalt(II)–copper(II) chain compounds **1b**–**3b**, in which the octahedral high-spin Co^{II} ions are orbitally degenerate ($^4T_{1g}$), we used the branch chain model developed by Drillon and coworkers for the related oxamato-bridged chain [CoCu(pbaOH)$(H_2O)_3$]·$2H_2O$.[18d] This model assumes that only z components of spin and orbital momenta are coupled and that the applied magnetic field is along the quantisation axis. The corresponding Hamiltonian is then expressed by Equation (2) in which i extends over the CoCu units, J and J' are the isotropic magnetic exchange and effective spin–orbit coupling parameters, respectively, Δ is the splitting of the T_1 orbital term of the Co^{II} ion into singlet and doublet orbital terms due to the axial symmetry. The orbital reduction (κ) is related to α according to $\alpha = -{}^3/_2\kappa$. Finally, g_{Co} and g_{Cu} are the Landé factors of the Co^{II} and Cu^{II} ions, respectively.

$$\mathbf{H} = \sum\nolimits_i [-J\mathbf{S}_{Co,i(z)}(\mathbf{S}_{Cu,i(z)} + \mathbf{S}_{Cu,i-1(z)}) + J'\mathbf{L}_{Co,i(z)}\mathbf{S}_{Co,i(z)} + \Delta\mathbf{L}_{Co,i(z)}{}^2 + (g_{Co}\mathbf{S}_{Co,i(z)} + g_{Cu}\mathbf{S}_{Cu,i(z)} + \alpha\mathbf{L}_{Co,i(z)})\beta\mathrm{H}_{(z)}] \quad (2)$$

The least-squares fit of the experimental data by this model in the temperature ranges of 45–290 (**1b** and **2b**) and 35–290 K (**3b**) confirmed the antiferromagnetic interaction through the oxamate bridges (see Table 5). The theoretical curves reproduce quite well the observed minima in the $\chi_M T$ versus T plots (solid lines in the inset in Figure 7a). The antiferromagnetic coupling between the Cu^{II} and Co^{II} ions through the oxamato bridge in **1b**–**3b** (Table 5) is somewhat weaker than that found in a related series of oxamato-bridged cobalt(II)–copper(II) chains ($-J = 35.0$–45.8 cm^{-1}).[11] The tetrahedral distortion from the ideal square-planar environment of the Cu^{II} ions in **1b**–**3b** accounts for these diferences. The effective spin–orbit coupling (J') can be related to the spin–orbit coupling parameter (λ) through the expression $J' = -{}^3/_2\kappa\lambda$. This gives values of λ in the range of -110 to -129 cm^{-1} ($\lambda = -180$ cm^{-1} for the free ion). The values of Δ for the high-spin Co^{II} ions in **1b**–**3b**

Table 5. Selected dc magnetic data for the $Co^{II}Cu^{II}$ chain compounds **1b**–**3b**.

Complex	$-J$ [cm^{-1}][a]	g_{Co}[b]	g_{Cu}[b]	$-\lambda$ [cm^{-1}][c]	κ[d]	Δ [cm^{-1}][e]
1b	31.0	2.41	2.10	129	0.82	600
2b	32.5	2.42	2.10	110	0.83	650
3b	19.5	2.38	2.10	126	0.83	590

[a] Intrachain magnetic coupling parameter. [b] Landé factor. [c] Spin–orbit coupling parameter (with $A = {}^3/_2$). [d] Orbital reduction parameter. [e] Axial orbital splitting parameter.

are similar to those reported for the aforementioned series of oxamato-bridged cobalt(II)–copper(II) chains ($\Delta = 538$–$719\ cm^{-1}$).[11] In a similar manner to what is observed for the parent family of copper(II)–manganese(II) chains, the magnetic coupling found for the racemic chain **3b** is weaker than the coupling obtained for the enantiopure chains **1b** and **2b**. This can be justified in similar terms to those used for the $Cu^{II}Mn^{II}$ chains.

Dynamic magnetic properties

Manganese(II)–copper(II) chains: The alternating current (ac) measurements for **1a**–**3a** showed no evidence of slow magnetic relaxation effects. In fact, no out-of-phase magnetic susceptibility signals (χ_M'') were observed above 2.0 K for these compounds (data not shown). This is likely due to the isotropic character of the octahedral high-spin Mn^{II} ion with a $^6A_1$ single-ion ground state (D value close to zero) and the very good isolation of the $Mn^{II}Cu^{II}$ chains, as revealed by the crystal structures of **1a**–**3a**.

Cobalt(II)–copper(II) chains: Although no slow relaxation effects were observed for the racemic compound **3b** above 2.0 K, the alternating current (ac) magnetic properties of the enantiopure cobalt(II)–copper(II) chain compounds **1b** and **2b** showed evidence of slow magnetic relaxation effects. This is reflected in Figure 8, which shows that χ_M'' is frequency-dependent below 4.0 K for **1b** and **2b**. This difference in the magnetic behaviour of the chiral and racemic compounds can be attributed to either the larger interchain interactions in **3b** or the lower value of J obtained from the fit of the magnetic data of **3b**. Despite the fact that the expected maxima of χ_M'' for **1b** and **2b** could not be observed down to 2.2 K (the limit of our susceptometer), this behaviour is typical of SCMs. Thus, under the assumption that an SCM has only one relaxation time (τ_0) with a characteristic activation energy (E_a) and considering that the adiabatic susceptibility is zero, it is possible to use Equation (3),[22] in which ω is the experimental ac field exciting frequency ($\omega = 2\pi\nu$), to roughly estimate the values of τ_0 and E_a.

$$\ln(\chi_M''/\chi_M') = \ln(\omega\tau_0) + E_a/k_B T \quad (3)$$

This method has already been applied to the evaluation of these factors in several SMMs in the literature.[22] The insets in Figure 8 show the fits of the experimental χ_M''/χ_M' data of compounds **1b** and **2b** by using Equation (3). The values obtained are $\tau_0 = 1.9(1)\times10^{-8}$ s and $E_a = 8.2(5)\ cm^{-1}$ for **1b** and $\tau_0 = 6.0(5)\times10^{-8}$ s and $E_a = 8.1(5)\ cm^{-1}$ for **2b**. Note that they are almost identical for both compounds and also that they lie within the range of those expected for a SCM.

To obtain a more accurate description and to confirm the values obtained by using Equation (3), measurements were carried out for compound **1b** at very low temperature.[23] The χ_M' and χ_M'' versus T plots for **1b** are shown in Figure 9; χ_M'' deviates from zero below 3.2 K and the expected frequency-dependent maxima vary from 1.8 K at 5700 Hz to 0.6 K at 0.11 Hz. Moreover, a second non-frequency-dependent peak in the ac susceptibility is observed at 0.4 K (Figure 9), which can be attributed to magnetic 3D ordering at these low temperatures. The variation in the temperature of the χ_M'' maxima (T_{max}) with the frequency of the oscillating field (ν), as expressed by the so-called Mydosh parameter (F)[24b] defined by Equation (4), is characteristic of single-chain magnet behaviour.

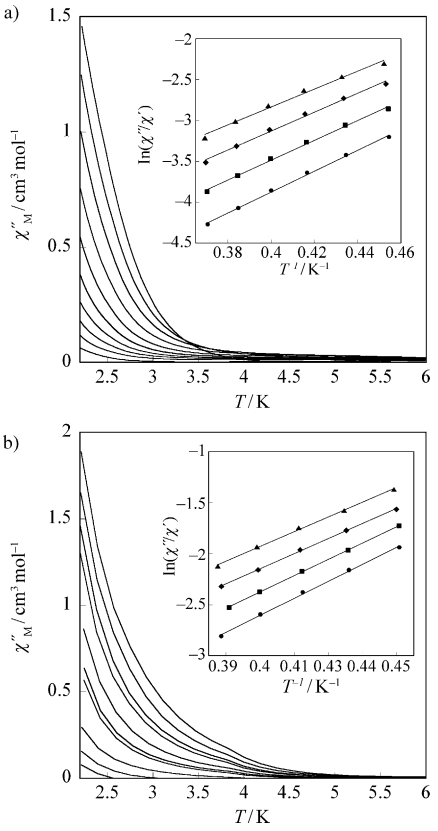

Figure 8. Temperature dependence of χ_M'' of a) **1b** and b) **2b** under zero applied static field at different frequencies (10–5878 Hz) of the ±1 G oscillating field. The insets show the natural logarithms of the χ_M''/χ_M' quotient versus $1/T$ for a) **1b** and b) **2b**.

$$F = (\Delta T_{max}/T_{max})/\Delta(\log\nu) \quad (4)$$

The calculated value of F of 0.21 is within the range expected for an SCM ($0.1 < F < 0.3$) supporting a single relaxation proecess and discarding a spin-glass behaviour ($F < 0.01$).[24] The relaxation time τ is calculated from the maximum in χ_M'' at a given frequency ν, at which it is assumed that switching of the oscillating ac field matches the relaxation rate of the magnetisation ($1/\tau = 2\pi\nu$). The calculated values of τ at T_{max} follow the Arrhenius law, characteristic of a thermally activated mechanism [Eq. (5); inset in Figure 9b], with an energy barrier (E_a) to reverse the magnetisation direction of 9.2 cm^{-1} and a pre-exponential factor (τ_0) of 2.2×10^{-8} s. These values are consistent with those previously reported for other oxamate-based SCMs[7–14] and are

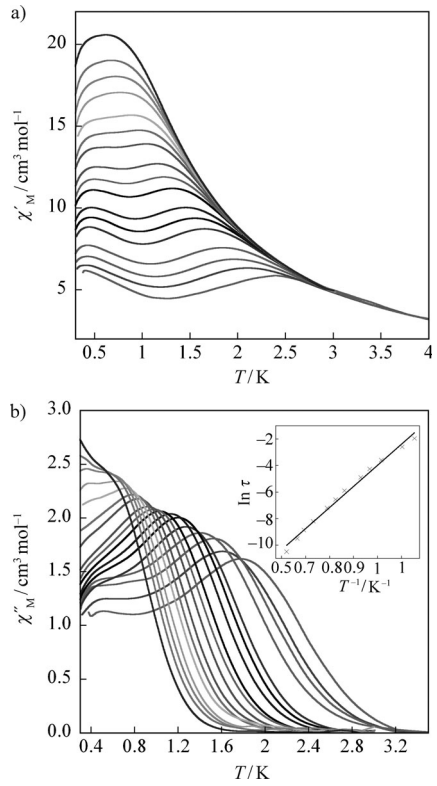

Figure 9. Temperature dependence of a) the in-phase and b) the out-of-phase magnetic susceptibilities of **1b** under zero applied static field at different frequencies (0.021–5700 Hz) of the ±1 G oscillating field. The inset shows the Arrhenius plot.

very close to those estimated by Equation (3) for compounds **1b** and **2b**. The Cole–Cole plot (Figure S5 in the Supporting Information) for **1b** shows an asymetrically distorted semi-circle shape due to the presence of the second peak below 1.0 K, as discussed above (Figure 9).

$$\tau = \tau_0 \exp\left(E_a/k_B T\right) \quad (5)$$

Conclusion

A new family of enantiopure heterobimetallic chains has been successfully synthesised by following a rationally designed self-assembly method consisting of the use of chiral mononuclear copper(II)–(*M*,*P*)-binaba complexes as bis-bidentate ligands with manganese(II) and cobalt(II) ions. By following this "complex-as-ligand" strategy, the chiral information contained in the configuration of the (*M*)- or (*P*)-binaba organic ligand (chiragen-type ligand) can be transferred to the stereochemistries of both the Cu^{II} and M^{II} centres in a controlled manner and consequently, the absolute configuration of the final $Cu^{II}M^{II}$ chain can be determined.[1e] This strategy has allowed the enantiopure chiral chains to be obtained that are made up of repeating units of the corresponding neutral chiral (*M*)-Cu^{II}-(Λ)-M^{II} [**1a** and **1b** with L = (*M*)-binaba] or (*P*)-Cu^{II}-(Δ)-M^{II} [**2a** and **2b** with L = (*P*)-binaba] motifs. In contrast, when using the racemic mononuclear copper(II)–binaba complex with manganese(II) or cobalt(II) ions, achiral zigzag $Cu^{II}M^{II}$ chains are obtained, that is, the $Cu^{II}M^{II}$ chain consists of alternating $[(M)\text{-}Cu^{II}\text{-}(\Lambda)\text{-}Mn^{II}]_n$ and $[(P)\text{-}Cu^{II}\text{-}(\Delta)\text{-}Mn^{II}]_n$ chains. From a magnetic point of view, both manganese(II)–copper(II) and cobalt(II)–copper(II) chains behave as ferrimagnetic chains with a moderately large intrachain antiferromagnetic coupling between the Cu^{II} and M^{II} (M = Mn and Co) ions through the oxamate bridge, in spite of the tetrahedral distortion of the copper(II) environment. Moreover, the closer proximity of the chains in **3a** compared with **1a** and **2a** is reflected in the magnetic behaviour. Thus, the achiral zigzag $Cu^{II}Mn^{II}$ chain **3a** shows significant antiferromagnetic interchain interactions as a consequence of the much shorter interchain Mn···Mn distance (ca. 1 Å). The same situation is found in the $Cu^{II}Co^{II}$ chains; the interchain interactions found in the racemic **3b** are not present in **1b** or **2b**. Therefore, different magnetic behaviour is observed for the enantiopure $Cu^{II}M^{II}$ chain compounds in comparison with the racemic compounds, not because of the optical properties but for structural reasons.

Interestingly, the enantiopure $Co^{II}Cu^{II}$ chains **1b** and **2b** show slow magnetic relaxation effects that are typical of SCMs. The observation of this phenomenon requires certain steric and magnetic requirements to be fulfilled. Indeed, the bulky organic ligand (*M*/*P*/*rac*)-binaba allows a good separation between the neighbouring chains and the oxamato fragment efficiently transmits the antiferromagnetic interaction between the copper(II) and cobalt(II) ions. These two features, together with the local magnetic anisotropy of the orbitally degenerate octahedral high-spin Co^{II} ions, allow the observation of the SCM behaviour. In the case of the racemic compound **3b**, the interchain magnetic interactions mentioned above preclude SCM behaviour. In contrast, slow relaxation of the magnetisation was observed for the first time in the enantiopure magnetic chain compounds **1b** and **2b** and thus they are the first examples of a new class of M_4 compounds, referred to as chiral single-chain magnets (CSCMs). The large magnetic moment due to the SCM behaviour of the 1D array of magnetic ions, which are also the chiral centres, ensures a strong coupling effect between the two physical properties, thus providing excellent possibilities for the study of the magnetochiral dichroism effect in enantiopure 1D compounds with a higher T_B.[2]

Experimental Section

Reagents: All chemicals were of reagent-grade quality and were purchased from commercial sources and used as received.

Preparation of the ligands H_2Et_2-(*M*)-binaba ($H_2Et_2L^1$), H_2Et_2-(*P*)-binaba ($H_2Et_2L^2$) and H_2Et_2-binaba ($H_2Et_2L^3$): The pro-ligand was prepared in a standard manner[25] by the condensation of the corresponding aromatic diamine [(*M*)-(+)-1,1′-binaphthyl-2,2′-diamine ($H_2Et_2L^1$), (*P*)-(−)-1,1′-binaphthyl-2,2′-diamine ($H_2Et_2L^2$) and 1,1′-binaphthyl-2,2′-diamine ($H_2Et_2L^3$)] (1.42 g, 5 mmol) and ethyl chlorooxoacetate (2.2 mL,

10 mmol) in THF (150 mL) at 0 °C under continuous stirring. The resulting solution was heated at reflux for 1 h and the solvent was removed in a rotatory evaporator to afford an oil that solidified when left at room temperature. The white solid obtained was filtered off, washed with a small amount of diethyl ether and dried under vacuum (see Table S1 in the Supporting Information).

Preparation of the mononuclear copper(II) complexes (nBu$_4$N)$_2$[Cu(L^1)]·2H$_2$O (1), (nBu$_4$N)$_2$[Cu(L^2)]·2H$_2$O (2) and (nBu$_4$N)$_2$[Cu(L^3)]·2H$_2$O (3): Complexes **1**–**3** were obtained by following a reported procedure[26] involving the reaction of the corresponding proligand ($H_2Et_2L^1$, $H_2Et_2L^2$ and $H_2Et_2L^3$; 0.48 g, 1 mmol) with $CuCl_2$·2H$_2$O (0.17 g, 1 mmol) and a solution of nBu$_4$NOH in methanol (1.0 M, 4 mL, 4 mmol) as a base in water. They were isolated as green polycrystalline solids, which were recrystallised in EtOH/ACN (1:1) at room temperature (see Table S2 in the Supporting Information).

Preparation of the heterobimetallic chain compounds

{Cu[(*M*)-binaba]Mn(DMSO)$_3$}·0.5DMSO·3H$_2$O (1a), {Cu[(*P*)-binaba]Mn(DMSO)$_3$}·0.5DMSO·3H$_2$O (2a) and {Cu[binaba]Mn(H$_2$O)-(DMSO)$_2$}·DMSO·H$_2$O (3a): Complexes **1a**–**3a** were prepared by using the same synthetic procedure. In a typical experiment, $Mn(NO_3)_2$·4H$_2$O (0.062 g, 0.25 mmol) was dissolved in hot DMSO (10 mL) at 70 °C and the solution was added dropwise to a solution of the corresponding tetrabutylammonium salt of the copper(II)–L^x (x = 1–3) precursor (0.25 mmol) dissolved in hot DMSO (10 mL). The resulting dark-green solution was filtered while hot and the filtrate was allowed to stand at room temperature. After several days, well-formed deep-green prisms of **1a**–**3a** appeared, which were filtered and air dried (see Table S2 in the Supporting Information).

{Cu[(*M*)-binaba]Co(DMF)$_2$}·DMF (1b), {Cu[(*P*)-binaba]Co-(DMF)$_2$}·DMF (2b) and {Cu[(*M*)-binaba]Co(DMF)$_2$}·2DMF (3b): Well-formed deep-green cubic prisms of **1b** and **2b** (suitable for single-crystal X-ray diffraction with synchrotron radiation) and a polycrystalline solid in the case of **3b** were obtained by slow diffusion in an H-shaped tube of a solution in DMF containing stoichiometric amounts of **1**–**3** (0.20 mmol) in one arm and $Co(NO_3)_2$·6H$_2$O (0.06 g, 0.20 mmol) in the other. They were isolated by filtration on paper and air dried (see Table S2 in the Supporting Information).

Physical techniques: Elemental analyses (C, H, Co, Cu, Mn, N) were performed at the Service Central d'Analyse du CNRS in Vernaisson (France). ^{1}H NMR spectra were recorded at room temperature on a Bruker AC 200 (200.1 MHz) spectrometer. [D$_6$]DMSO was used as the solvent and internal standard (δ = 2.50 ppm). IR spectra were recorded on a Bio-Rad FTS165 spectrophotometer in KBr pellets. Natural circular dichroism (NCD) curves were recorded by using a Jasco model J-810 spectropolarimeter. Complexes **1a**, **2a**, **1b** and **2b** (1 mg) and KBr (120 mg) were mixed and pressed as pellets. The spectra were normalised and corrected for baseline deviation to enable comparison. Variable-temperature (2.0–300 K) dc magnetic susceptibility measurements were carried out on polycrystalline samples of **1a**–**3a** and **1b**–**3b** with a Quantum Design SQUID magnetometer. The magnetic data were corrected for the diamagnetism of the constituent atoms and the sample holder. Low-temperature ac susceptibility measurements for **1b** were performed with a SQUID magnetometer equipped with a miniature dilution refrigerator developed at the CRTBT-CNRS in Grenoble. Vacuum grease was mixed with **1b** and pressed into a small copper pouch to ensure good thermal contact at low temperature.

Crystal structure data collection and refinement: The structures of **1a**–**3a**, **1b** and **2b** were solved by direct methods and refined by full-matrix least-squares methods on F^2 by using the SHELXS-97[27a] and SHELXL-97[27a] programs. Data were collected for **1a**, **1b** and **2b** in the BM16 beamline at the ESRF (Grenoble, France) and indexed, integrated and scaled by using the HKL2000 program[27b] with data being collected for **2a** and **3a** by using a Nonius–KappaCCD diffractometer with graphite-monochromated $Mo_{K\alpha}$ radiation with data reduction performed with the COLLECT[27c] and EVALCCD[27d] programs. All calculations for data reduction, structure solution and refinement were performed by using standard procedures (WINGX).[27f] The final geometrical calculations and graphical manipulations were performed with the PARST97[27g] and CRYSTAL MAKER[27h] programs, respectively. The hydrogen atoms of the organic ligand and the DMF and DMSO molecules were located at calculated positions and refined with isotropic thermal parameters, whereas those of the water molecules were neither found nor calculated. Partial occupation factors were assigned by a preliminary refinement of the s.o.f. parameter, which was restrained to this value in subsequent refinements. A summary of the crystallographic data for **1a**–**3a**, **1b** and **2b** are listed in Table 1.

CCDC-825207 (**1a**), 825208 (**2a**), 825209 (**3a**), 720897 (**1b**) and 825210 (**2b**) contain the supplementary crystallographic data for this paper. These data can be obtained free of charge from The Cambridge Crystallographic Data Centre via www.ccdc.cam.ac.uk/data_request/cif.

Acknowledgements

This work was supported by the MICINN of Spain (Projects CTQ2010-15364, MAT2010-19681, DPI2010-21103-C04-03, CSD2007-00010 and CSD2006-00015), the Generalitat Valenciana (Project PROMETEO/2009/108), the ACIISI-Gobierno Autónomo de Canarias (Project PIL-2070901 and structuring project NANOMAC), the MFR, the CNRS (France) and the European Union through the Magmanet Network of Excellence (Contract 03/197). We also aknowledge the Long Term Project HS3902 of the ESRF, Grenoble, France, for the beamtime assigned. J.F.-S. thanks the Generalitat Valenciana for a doctoral grant. E.P. and J.P. thank the "Juan de la Cierva" (MICINN) and the structuring project NANOMAC, respectively, for postdoctoral contracts. We are especially indebted to Dr. Rafael Ruiz-García for unselfish help, stimulating talks and continuous interest in this work.

[1] a) O. Sato, *Acc. Chem. Res.* **2003**, *36*, 692; b) Y. Arimoto, S. Ohkoshi, Z. J. Zhong, H. Seino, Y. Mizobe, K. Hashomoto, *J. Am. Chem. Soc.* **2003**, *125*, 9240; c) G. Li, T. Akitsu, O. Sato, Y. Einaga, *J. Am. Chem. Soc.* **2003**, *125*, 12396.

[2] a) K. Takahashi, T. Kawakami, Z. Gu, Y. Einaga, A. Fujishima, O. Sato, *Chem. Commun.* **2003**, 2374; b) G. J. Halder, C. J. Kepert, B. Moubaraki, K. S. Murray, J. D. Cashion, *Science* **2002**, *298*, 1762; c) V. Niel, A. L. Thompson, M. C. Munoz, A. Galet, A. E. Goeta, J. A. Real, *Angew. Chem.* **2003**, *115*, 3890; *Angew. Chem. Int. Ed.* **2003**, *42*, 3760.

[3] a) E. Coronado, J. R. Galan-Mascaros, C. J. Gomez-Garcia, V. Laukhin, *Nature* **2000**, *408*, 447; b) E. Coronado, J. R. Galan-Mascaros, *J. Mater. Chem.* **2005**, *15*, 66; c) E. Coronado, P. Day, *Chem. Rev.* **2004**, *104*, 5419.

[4] a) K. Inoue, K. Kikuchi, M. Ohba, H. Okawa, *Angew. Chem.* **2003**, *115*, 4857; *Angew. Chem. Int. Ed.* **2003**, *42*, 4709; b) K. Inoue, H. Imai, P. S. Ghalsasi, K. Kikuchi, M. Ohba, H. Okawa, J. V. Yakhmi, *Angew. Chem.* **2001**, *113*, 4372; *Angew. Chem. Int. Ed.* **2001**, *40*, 4242; c) E. Coronado, J. R. Galan-Mascaros, C. J. Gomez-Garcia, J. M. Martinez-Agudo, *Inorg. Chem.* **2001**, *40*, 113; d) O. Mamula, A. von Zelewsky, T. Bark, H. Stoeckli-Evans, A. Neels, G. Bernardinelli, *Chem. Eur. J.* **2000**, *6*, 3575.

[5] a) C. Train, R. Gheorghe, V. Krstic, L. M. Chamoreau, N. S. Ovanesyan, G. L. J. A. Rikken, M. Gruselle, M. Verdaguer, *Nat. Mater.* **2008**, *7*, 729; b) G. L. J. A. Rikken, E. Raupach, *Nature* **1997**, *390*, 493.

[6] M. M. Turnbull, T. Sugimoto, L. K. Thompson, *Molecule-Based Magnetic Materials*, ACS, Washington, **1996**.

[7] a) R. Lescouëzec, L. M. Toma, J. Vaissermann, M. Verdaguer, F. S. Delgado, C. Ruiz-Pérez, F. Lloret, M. Julve, *Coord. Chem. Rev.* **2005**, *249*, 2691; b) L. Bogani, A. Vindigni, R. Sessoli, D. Gatteschi, *J. Mater. Chem.* **2008**, *18*, 4750; c) H. Miyasaka, M. Julve, M. Yamashita, R. Clérac, *Inorg. Chem.* **2009**, *48*, 3420; d) H. L. Sun, Z. M. Wang, S. Gao, *Coord. Chem. Rev.* **2010**, *254*, 1081.

[8] a) A. Caneschi, D. Gatteschi, N. Lalioti, C. Sangregorio, R. Sessoli, G. Venturi, A. Vindigni, A. Rettori, M. G. Pini, M. Novak, *Angew.*

Chem. **2001**, *113*, 1810; *Angew. Chem. Int. Ed.* **2001**, *40*, 1760; b) L. Bogani, C. Sangregorio, R. Sessoli, D. Gatteschi, *Angew. Chem.* **2005**, *117*, 5967; *Angew. Chem. Int. Ed.* **2005**, *44*, 5817; c) K. Bernot, L. Bogani, A. Caneschi, D. Gatteschi, R. Sessoli, *J. Am. Chem. Soc.* **2006**, *128*, 7947.

[9] a) R. Clérac, H. Miyasaka, M. Yamashita, C. Coulon, *J. Am. Chem. Soc.* **2002**, *124*, 12837; b) H. Miyasaka, R. Clérac, K. Mizushima, K. Sugiura, M. Yamashita, W. Wernsdorfer, C. Coulon, *Inorg. Chem.* **2003**, *42*, 8203; c) A. Saitoh, H. Miyasaka, M. Yamashita, R. Clérac, *J. Mater. Chem.* **2007**, *17*, 2002; d) H. Miyasaka, A. Saitoh, M. Yamashita, R. Clérac, *Dalton Trans.* **2008**, 2422; e) M. Ferbinteanu, H. Miyasaka, W. Wernsdorfer, K. Nakata, K. Sugiura, M. Yamashita, C. Coulon, R. Clérac, *J. Am. Chem. Soc.* **2005**, *127*, 3090; f) H. Miyasaka, T. Madanbashi, K. Sugimoto, Y. Nakazawa, W. Wernsdorfer, K. Sugiura, M. Yamashita, C. Coulon, R. Clérac, *Chem. Eur. J.* **2006**, *12*, 7028.

[10] a) R. Lescouëzec, J. Vaissermann, C. Ruiz-Pérez, F. Lloret, R. Carrasco, M. Julve, M. Verdaguer, Y. Dromzée, D. Gatteschi, W. Wernsdorfer, *Angew. Chem.* **2003**, *115*, 1521; *Angew. Chem. Int. Ed.* **2003**, *42*, 1483; b) L. M. Toma, R. Lescouëzec, F. Lloret, M. Julve, J. Vaissermann, M. Verdaguer, *Chem. Commun.* **2003**, 1850; c) L. M. Toma, F. S. Delgado, C. Ruiz-Pérez, R. Carrasco, J. Cano, F. Lloret, M. Julve, *Dalton Trans.* **2004**, 2836; d) L. M. Toma, R. Lescouëzec, J. Pasán, C. Ruiz-Pérez, J. Vaissermann, J. Cano, R. Carrasco, W. Wernsdorfer, F. Lloret, M. Julve, *J. Am. Chem. Soc.* **2006**, *128*, 4842; e) L. M. Toma, R. Lescouëzec, S. Uriel, R. Llusar, C. Ruiz-Pérez, J. Vaissermann, F. Lloret, M. Julve, *Dalton Trans.* **2007**, 3690.

[11] a) E. Pardo, R. Ruiz-García, F. Lloret, J. Faus, M. Julve, Y. Journaux, F. S. Delgado, C. Ruiz-Pérez, *Adv. Mater.* **2004**, *16*, 1597; b) E. Pardo, R. Ruiz-García, F. Lloret, J. Faus, M. Julve, Y. Journaux, M. A. Novak, F. S. Delgado, C. Ruiz-Pérez, *Chem. Eur. J.* **2007**, *13*, 2054; c) E. Pardo, C. Train, R. Lescouëzec, Y. Journaux, J. Pasán, C. Ruiz-Pérez, F. S. Delgado, R. Ruiz-García, F. Lloret, C. Paulsen, *Chem. Commun.* **2010**, *46*, 2322; d) J. Ferrando-Soria, E. Pardo, R. Ruiz-García, J. Cano, F. Lloret, M. Julve, Y. Journaux, J. Pasán, C. Ruiz-Pérez, *Chem. Eur. J.* **2011**, *17*, 2176.

[12] a) S. Wang, J.-L. Zuo, S. Gao, Y. Song, H.-C. Zhou, Y.-Z. Zhang, X.-Z. You, *J. Am. Chem. Soc.* **2004**, *126*, 8900; b) H. R. Wen, C.-F. Wang, Y. Song, J.-L. Zuo, X.-Z. You, *Inorg. Chem.* **2006**, *45*, 8942.

[13] E. Coronado, J. R. Galan-Mascaros, C. Martí-Gastaldo, *J. Am. Chem. Soc.* **2008**, *130*, 14987.

[14] N. Hoshino, Y. Sekine, M. Nihei, H. Oshio, *Chem. Commun.* **2010**, *46*, 6117.

[15] R. J. Glauber, *J. Math. Physics* **1963**, *4*, 294.

[16] a) R. E. P. Winpenny, *Adv. Inorg. Chem.* **2001**, *52*, 1; b) D. Gatteschi, R. Sessoli, *Angew. Chem.* **2003**, *115*, 278; *Angew. Chem. Int. Ed.* **2003**, *42*, 268; c) L. Thomas, F. Lionti, R. Ballou, D. Gatteschi, R. Sessoli, B. Barbara, *Nature* **1996**, *383*, 145; d) J. R. Friedman, M. P. Sarachik, J. Tejada, R. Ziolo, *Phys. Rev. Lett.* **1996**, *76*, 3830; e) C. Coulon, R. Clérac, L. Lecren, W. Wernsdorfer, H. Miyasaka, *Phys. Rev. B* **2004**, *69*, 132408.

[17] a) H. O. Stumpf, C. L. M. Pereira, A. C. Doriguetto, C. Konzen, L. C. B. Meira, N. G. Fernandes, Y. P. Mascarenhas, J. Ellena, M. Knobel, *Eur. J. Inorg. Chem.* **2005**, 5018; b) H. O. Stumpf, Y. Pei, L. Ouahab, F. Leberre, E. Codjovi, O. Kahn, *Inorg. Chem.* **1993**, *32*, 5687; c) H. O. Stumpf, Y. Pei, O. Kahn, J. Sletten, J. P. Renard, *J. Am. Chem. Soc.* **1993**, *115*, 6738.

[18] a) M. Verdaguer, A. Gleizes, J. P. Renard, J. Seiden, *Phys. Rev. B* **1984**, *29*, 5144; b) Y. Pei, O. Kahn, J. Sletten, J. P. Renard, R. Georges, J. C. Gianduzzo, J. Curely, Q. Xu, *Inorg. Chem.* **1988**, *27*, 47; c) R. Georges, J. Curely, J. C. Gianduzzo, X. Qiang, O. Kahn, Y. Pei, *Physica B+C* **1988**, *153*, 77; d) P. J. Van Koningsbruggen, O. Kahn, K. Nakatani, Y. Pei, J. P. Renard, M. Drillon, P. Legoll, *Inorg. Chem.* **1990**, *29*, 3325.

[19] a) J. Cano, P. Alemany, S. Alvarez, M. Verdaguer, E. Ruiz, *Chem. Eur. J.* **1998**, *4*, 476; b) J. Cano, E. Ruiz, P.e Alemany, F. Lloret, S. Alvarez, *Dalton Trans.* **1999**, 1699.

[20] a) J. M. Herrera, A. Bleuzen, Y. Dromzee, M. Julve, F. Lloret, M. Verdaguer, *Inorg. Chem.* **2003**, *42*, 7052; b) F. Lloret, M. Julve, J. Cano, R. Ruiz-García, E. Pardo, *Inorg. Chim. Acta* **2008**, *361*, 3432.

[21] a) J. Cernak, K. A. Abboud, *Acta Crystallogr. Sect. C* **2000**, *56*, 783; b) E. Colacio, M. Ghazi, R. Kivekas, M. Klinga, F. Lloret, J. M. Moreno, *Inorg. Chem.* **2000**, *39*, 2770; c) G. C. Guo, Q. M. Wang, T. C. Mak, W. Inorg, *Chem. Commun.* **2000**, 313; d) B. F. Abrahams, K. D. Lu, B. Moubaraki, K. S. Murray, R. Robson, *Dalton Trans.* **2000**, 1793; e) Y. B. Dong, M. D. Smith, H. C. Zur Loye, *Inorg. Chem.* **2000**, *39*, 1943; f) E. Colacio, J. M. Dominguez-Vera, M. Ghazi, R. Kivekas, J. M. Moreno, A. Pajunen, *Dalton Trans.* **2000**, 505; g) M. Maekawa, K. Sugimoto, T. Kuroda-Sowa, Y. Suenaga, M. Munakata, *Dalton Trans.* **1999**, 4357; h) E. Colacio, J. M. Domínguez-Vera, M. Ghazi, R. Kivekas, M. Klinga, J. M. Moreno, *Eur. J. Inorg. Chem.* **1999**, 441; i) M. Mimura, T. Matsuo, T. Nakashima, N. Matsumoto, *Inorg. Chem.* **1998**, *37*, 3553; j) Z. M. Sun, P. K. Gantzel, D. N. Hendrickson, *Polyhedron* **1998**, *17*, 1511; k) F. B. Stocker, M. A. Troester, D. Britton, *Inorg. Chem.* **1996**, *35*, 3145.

[22] a) F. Luis, J. Bartolomé, J. F. Fernández, J. Tejada, J. M. Hernández, X. X. Zhang, R. Ziolo, *Phys. Rev. B* **1997**, *55*, 11448; b) J. Bartolomé, G. Filoti, V. Kuncser, G. Schinteie, V. Mereacre, C. E. Anson, A. K. Powell, D. Prodius, C. Turta, *Phys. Rev. B* **2009**, *80*, 014430.

[23] The magnetic properties of only one of the two CuCo chain compounds was measured at a very low temperature ($T<2$ K) as they are non-superimposable mirror images of each other and their magnetic properties must be the same.

[24] a) M. A. Girtu, C. M. Wynn, W. Fujita, K. Awaga, A. Epstein, *J. Phys. Rev. B* **1998**, *57*, R11058; b) J. A. Mydosh, *Spin Glasses: An Experimental Introduction*, Taylor & Francis, London, **1993**; c) D. Chowdhury, *Spin Glasses and Other Frustrated Systems*, Princeton University Press, New Jersey, **1986**; d) K. Moorjani, J. M. Coey, *Magnetic Glasses*, Elsevier, New York, **1984**; e) K. Binder, A. P. Young, *Rev. Mod. Phys.* **1986**, *58*, 801.

[25] B. Cervera, J. L. Sanz, M. J. Ibáñez, G. Villa, F. Lloret, M. Julve, R. Ruiz, X. Ottenwaelder, A. Aukauloo, S. Poussereau, Y. Journaux, M. C. Muñoz, *J. Chem. Soc. Dalton Trans.* **1998**, 781.

[26] B. Bräuer, F. Weigend, M. Fittipaldi, D. Gatteschi, E. J. Reijerse, A. Guerri, S. Ciattini, G. Salvan, T. Rüffer, *Inorg. Chem.* **2008**, *47*, 6633.

[27] a) SHELX97, Programs for Crystal Structure Analysis (Release 97-2), G. M. Sheldrick, Institüt für Anorganische Chemie der Universität, Göttingen (Germany), **1998**; b) Z. Otwinowski, W. Minor, *Processing of X-ray Diffraction Data Collected in Oscillation Mode Methods in Enzymology, Vol. 276: Macromolecular Crystallography, Part A* (Eds.: C. W. Carter, Jr., R. M. Sweet), Academic Press, pp. 307–326, **1997**; c) COLLECT, R. W. W. Hooft, Nonius BV, Delft, **1999**; d) A. J. M. Duisenberg, L. M. J. Kroon-Batenburg, A. M. M. Schreurs, *J. Appl. Crystallogr.* **2003**, *36*, 220 (EVALCCD); e) SADABS, version 2.03, Bruker AXS Inc., Madison, **2000**; f) WINGX: L. J. Farrugia, *J. Appl. Cryst.* **1999**, *32*, 837; g) M. Nardelli, *J. Appl. Crystallogr.* **1995**, *28*, 659; h) CRYSTAL MAKER, D. Palmer, Cambridge University Technical Services, Cambridge, **1996**.

Received: May 12, 2011
Revised: July 27, 2011
Published online: September 19, 2011

